ADVANCES IN ATMOSPHERIC SCIENCES, VOL. 35, AUGUST 2018, 942–954

• **Original Paper** •

Assessment and Assimilation of FY-3 Humidity Sounders and Imager in the UK Met Office Global Model

Fabien CARMINATI*, Brett CANDY, William BELL†, and Nigel ATKINSON

UK Met Office, Exeter EX1 3PB*, UK*

(Received 27 October 2017; revised 7 March 2018; accepted 7 March 2018)

ABSTRACT

China's FengYun 3 (FY-3) polar orbiting satellites are set to become an important source of observational data for numerical weather prediction (NWP), atmospheric reanalyses, and climate monitoring studies over the next two decades. As part of the Climate Science for Service Partnership China (CSSP China) program, FY-3B Microwave Humidity Sounder 1 (MWHS-1) and FY-3C MWHS-2 observations have been thoroughly assessed and prepared for operational assimilation. This represents the first time observations from China's polar orbiting satellites have been used in the UK's global NWP model. Since 2016, continuous data quality monitoring has shown occasional bias changes found to be correlated to changes in the energy supply scheme regulating the platform heating system and other transient anomalies. Nonetheless, MWHS-1 and MWHS-2 significantly contribute to the 24-h forecast error reduction by 0.3% and 0.6%, respectively, and the combination of both instruments is shown to improve the fit to the model background of independent sounders by up to 1%. The observations from the Microwave Radiation Imager (MWRI) also are a potentially significant source of benefits for NWP models, but a solar-dependent bias observed in the instrument half-orbits has prevented their assimilation. This paper presents the bases of a correction scheme developed at the Met Office for the purpose of a future assimilation of MWRI data.

Key words: Microwave Humidity Sounder, Microwave Radiation Imager, numerical weather prediction

Citation: Carminati, F., B. Candy, W. Bell, and N. Atkinson, 2018: Assessment and assimilation of FY-3 humidity sounders and imager in the UK Met Office global model. *Adv. Atmos. Sci.*, **35**(8), 942–954, https://doi.org/10.1007/s00376-018-7266-8.

1. Introduction

With the FengYun (FY) program, China is becoming the third pillar of the satellite-based Earth Observation System along with the USA and Europe. The FY program started in 1988 with the first generation of Chinese polar-orbiting satellite and is now composed of an operational fleet of polar-orbiting platforms of second generation (FY-3) and geostationary satellites (Li, 2001; Meng, 2004).

Spaceborne observations are widely used in the production of climate data records (Christy et al., 1998; Yang et al., 2016) and regional or global reanalyses (Uppala et al., 2005). A fundamental step in the production of such records is the detailed characterization of data quality for existing and new instruments. The rigorous assessment of instrument biases, which include radiometer nonlinearity, channel frequency offset or drift, calibration error, or solar thermal effects, typically lasts several decades when conventional observation-based techniques are employed. For example, spectral shifts in the channel frequencies of the microwave sounding unit (MSU) instruments, which flew between 1978 and 2007 on 10 different NOAA platforms, were not identified until a recent model-based study by Lu and Bell (2014), more than four decades after the launch of the first MSU.

In recent years, the overall process has been accelerated using numerical weather prediction (NWP) models to characterize satellite radiance biases (Saunders et al., 2013b). The data assimilation (DA) systems in NWP models provide a high-quality framework for the analysis of satellite observations thanks to a continuous, global, and homogeneous representation of the atmosphere that standard conventional networks cannot provide by nature. DA systems ingest an extremely large number of spaceborne, airborne, ground-based (and oceanic for coupled models) remote or in-situ measurements that drive down NWP analysis and forecast errors. It is commonly assumed that the state-of-the-art NWP models can represent top-of-the-atmosphere radiances at frequencies sensitive to mid-tropospheric temperature with an accuracy of the order of 0.1 K and at frequencies sensitive to humidity within the range of 0.5–1 K. These estimations have been established from multi-model and double comparisons studies, which have highlighted global or local patterns inherent to

* Corresponding author: Fabien CARMINATI
Email: Fabien.carminati@metoffice.gov.uk
† Now at ECMWF, Reading, UK

instrument-related biases of that order of magnitude (Bell et al., 2008; Doherty et al., 2012; Bormann et al., 2013; Lu and Bell, 2014). The bias characterization studies of the Chinese instruments of early FY-3 missions are successful examples of NWP-based applications (Lu et al., 2011a, 2011b, Zou et al., 2011).

Building on a mature collaboration between the Met Office and the China Meteorological Administration-National Satellite Meteorological Center (CMA-NSMC) developed through the Climate Science for Service Partnership China (CSSP China), the delay between launch and successful application in climate services for the Chinese instruments of the FY-3 series is aimed to be reduced to less than a decade. In that regard, the first three years of "CSSP China Work Package 1: Monitoring, Attribution, and Reanalysis" have focused on the evaluation of data quality from the most recent of the FY-3 missions: FY-3B and FY-3C. Detailed assessment of the FY-3B Microwave Humidity Sounder 1 (MWHS-1), its advanced version FY-3C MWHS-2, and the FY-3C Microwave Radiation Imager (MWRI), have been reported in CSSP China key deliverable reports (Lu et al., 2015; Lawrence et al., 2017). The findings have been fed back to the CMA for an efficient and timely redesign, correction, and/or recalibration of the instruments.

The incorporation of FY-3B MWHS-1 and FY-3C MWHS-2 data in the Met Office operational global NWP model in 2016 has been the next step and a significant milestone for the FY-3 program. The continuous operational global monitoring of those instruments has allowed the rapid feedback to the CMA of anomalies in the data, whilst their assimilation in operation has significantly benefited the Met Office global forecast system. In parallel, the development and assessment of a bias correction for MWRI observations has been ongoing at the Met Office.

This paper provides insights into MWHS-1 and MWHS-2 assimilation in operation and the impact on the Met Office global system, and reports on MWRI bias correction advancements as follows. Section 2 details the instrument characteristics; section 3 introduces the progress on MWRI assessment and bias correction; section 4 presents the data processing system at the Met Office, MWHS-1 and MWHS-2 data quality and monitoring in operation, and their impact on the system; section 5 concludes the study.

2. Instrument characteristics

2.1. *FY-3B MWHS-1*

MWHS-1 is a five-channel cross-track scanning radiometer, launched for the first time onboard the FY-3A platform in 2008 and then onboard FY-3B in 2010 on an afternoon orbit [1445 Equator Crossing Time (ECT), ascending node] (Dong et al., 2009). With two window channels at 150 GHz and three channels sounding the water vapor line at 183 GHz, the MWHS-1 sounding capability is comparable with, although not identical to, the Microwave Humidity Sounder (MHS) (Kleespies and Watts, 2006), as shown in Table 1. The MWHS-1 scanning geometry provides cross-track scans of 98 16-km steps (at nadir) for a total swath of about 2600 km and an instantaneous field of view on the surface at nadir of approximately 16 km. Channels 3, 4 and 5 peak in the upper, mid and lower troposphere, respectively, allowing between two and three pieces of independent information in the vertical direction.

The quality of MWHS-1 data has been assessed by Lu et al. (2011b) and Chen et al. (2015). In both studies, data were found of matching quality with those of the MHS, although observations from MWHS-1 have a random noise 0.8–1 K greater than that from the MHS. They also reported a scanning-angle bias of complex modulations, varying with the channel frequencies, reaching up to 2 K peak-to-peak amplitude.

Table 1. MWHS-1, MWHS-2, ATMS and MHS channel frequencies and polarization (V, vertical; H, horizontal) at nadir.

Channel number				Frequency (GHz) and polarization			
MWHS-1	MWHS-2	MHS	ATMS	MWHS-1	MWHS-2	MHS	ATMS
-	1	1	16	-	89 (H)	89 (V)	88.2 (V)
-	2	-	-	-	118.75 ± 0.08 (V)	-	-
-	3	-	-	-	118.75 ± 0.2 (V)	-	-
-	4	-	-	-	118.75 ± 0.3 (V)	-	-
-	5	-	-	-	118.75 ± 0.8 (V)	-	-
-	6	-	-	-	118.75 ± 1.1 (V)	-	-
-	7	-	-	-	118.75 ± 2.5 (V)	-	-
-	8	-	-	-	118.75 ± 3.0 (V)	-	-
-	9	-	-	-	118.75 ± 5.0 (V)	-	-
1	-	2	-	150 (V)	-	157 (V)	-
2	10	-	17	150 (H)	150 (H)	-	165 (H)
3	11	3	22	183 ± 1.0 (V)	183 ± 1.0 (V)	183 ± 1.0 (H)	183 ± 1.0 (H)
-	12	-	21	-	183 ± 1.8 (V)	-	183 ± 1.8 (H)
4	13	4	20	183 ± 3.0 (V)	183 ± 3.0 (V)	183 ± 3.0 (H)	183 ± 3.0 (H)
-	14	-	19	-	183 ± 4.5 (V)	-	183 ± 4.5 (H)
5	15	5	18	183 ± 7.0 (V)	183 ± 7.0 (V)	190.31 (V)	183 ± 7.0 (H)

Similar conclusions have been drawn from an internal evaluation conducted at the Met Office. However, a scene temperature dependency was also observed in MWHS-1 observations, not reported in the studies referred to previously. The cause of this bias variation with scene temperature is not known. Figure 1 illustrates this scene temperature dependency for one day of background departure (i.e., the difference observation-minus-model background, referred to as innovation or O-B). The background is computed from the short-range forecasts (T+6) from the Met Office global model interpolated at the location and time of the observation and processed through the fast radiative transfer model RTTOV version 11 (Saunders et al., 2013a). Data are from 13 December 2016, quality-controlled (left), quality-controlled and corrected (right), as in operation (see section 4.1). In the most densely populated segment, between 260 and 280 K, the O-Bs increase by 0.1 K for every 1 K increase in scene temperature. The slope in that segment disappears in the corrected dataset, attesting of the bias correction scheme efficiency.

2.2. *FY-3C MWHS-2*

MWHS-2 is an advanced version of MWHS-1 and was launched in 2013 onboard FY-3C on a morning orbit (1015 ECT, descending node). The instrument has sounding capability in the 183 GHz water vapor band (five channels), in the window frequencies at 89 and 150 GHz (two channels), and a unique set of eight channels in the 118 GHz oxygen band improving the instrument sensitivity to humidity, temperature, and ice particles (Li et al., 2016). The MWHS-2 window and 183 GHz channels are similar to those of the Advanced Technology Microwave Sounder (ATMS) (Muth et al., 2004), as shown in Table 1. Like its predecessor, the instrument has 98 steps across track, with a resolution of 16 km at nadir for the 183 GHz channels and 32 km at nadir for the window and 118 GHz channels.

The present study focuses on MWHS-2 183 GHz frequencies, as they are the channels assimilated in operation at the Met Office. The quality assessment of those channels has been reported by Lawrence et al. (2015), Lu et al. (2015), and Li et al. (2016). The quality of MWHS-2 data was found to be comparable with that of ATMS, with mean global biases of the same magnitude, albeit slightly larger and (for some channels) of opposite sign. The noise and scanning-angle biases were shown to be comparable for both instruments, apart from more variability in ATMS data. A low-magnitude striping similar to or smaller than that of ATMS has been observed in MWHS-2 data.

2.3. *FY-3C MWRI*

MWRI is a microwave conical-scanning imager that measures frequencies at 10.65, 18.7, 23.8, 36.5 and 89 GHz both in vertical polarization (V-pol) and horizontal polarization (Yang et al., 2011). MWRI is part of the payload of all FY-3 platforms launched to date, although FY-3A MWRI failed soon after launch in 2008. The instrument shares frequencies with other imagers, including the Advanced Microwave Scanning Radiometer-2 (AMSR-2) (Imaoka et al., 2010), but has a new design that provides an improved calibration method, as described by Yang et al. (2011). This calibration system relies on a main reflector that is common to the Earth, cold and warm views, in addition to two independent reflectors exclusively used for the cold and warm targets. The aim was to avoid the solar-dependent biases that used to affect past imagers (Bell et al., 2008; Geer et al., 2010) whose calibration could not account for the emissions due to the sun-heated main reflector. Table 2 summarizes the instrument characteristics.

An assessment of FY-3C MWRI has been provided by Lawrence et al. (2017). The authors compared observations to short-range forecasts from both the ECMWF and Met Office global models. They concluded that MWRI suffers a 2 K bias between the ascending and descending half-orbits, consistent across all channels, with complex geographical patterns. Although the calibration excludes the main reflector

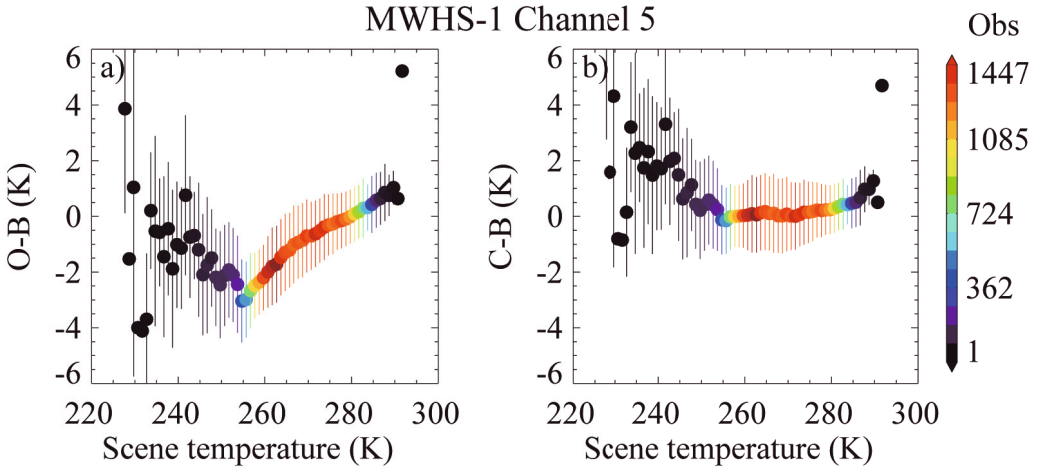

Fig. 1. MWHS-1 channel 5 observations-minus-background (a) before correction (O-B) and (b) after correction (C-B) as a function of the scene temperature (right). The color illustrates the number of observations per 1 K bin. Vertical bars show the 1σ standard deviation.

Table 2. MWRI and AMSR-2 channel frequencies, polarization (V, vertical; H, horizontal), and bandwidth.

Channel number		Frequency (GHz) and polarization		Bandwidth (MHz)	
MWRI	AMSR-2	MWRI	AMSR-2	MWRI	AMSR-2
1	5	10.65 (V)	10.65 (V)	180	100
2	6	10.65 (H)	10.65 (H)	180	100
3	7	18.7 (V)	18.7 (V)	200	200
4	8	18.7 (H)	18.7 (H)	200	200
5	9	23.8 (V)	23.8 (V)	400	400
6	10	23.8 (H)	23.8 (H)	400	400
7	11	36.5 (V)	36.5 (V)	400	1000
8	12	36.5 (H)	36.5 (H)	400	1000
9	13	89 (V)	89 (V)	3000	3000
10	14	89 (H)	89 (H)	3000	3000

as a source of emissions inducing this bias, it is possible that other parts of the instrument, such as the calibration mirrors, contribute to it. It was also suggested that the contamination of the warm load by the Earth scene, as described by Yang et al. (2011), might not be fully removed and also contributes to the bias.

The assessment also showed that MWRI is affected by television radio frequency interference (TFI) at 10.65 and 18.7GHz. TFI affects the channels overlapping with unprotected parts of the spectrum used by geostationary telecommunication satellites, whose signals bounce back from the ocean surface and contaminate the instrument observations.

These findings are in line with the work of Zou et al. (2014) and Tian and Zou (2016), who reported TFI affecting AMSR-E and AMSR-2 observations at similar frequencies and locations. This also complements the work of Zou et al. (2012), who showed that FY-3B MWRI is subject to RFI (radio frequency interference) from active ground-based transmitters used for military and civil applications.

These biases are a challenge for NWP centers wishing to assimilate the MWRI data. In particular, the ascending–descending bias requires a correction scheme with orbital angle-based predictors similar to that developed for the Special Sensor Microwave Imager/Sounder (SSMIS) by Booton et al. (2013). Such a scheme is under development at the Met Office and further discussed in the next section.

3. MWRI correction scheme

As shown by Lawrence et al. (2017), the FY-3C MWRI shows a distinct ascending–descending bias across all channels of up to 2 K. An example can be seen in Fig. 2, in which histograms for 24 hours of data show the difference between MWRI channel 5 observations (23.8 GHZ V-pol) and the NWP background for ascending and descending orbits. A 1.5 K shift in the mean of the distributions is observed, with the nighttime (ascending) warmer than the daytime (descending) observations.

To remove the complex variation in instrument bias along

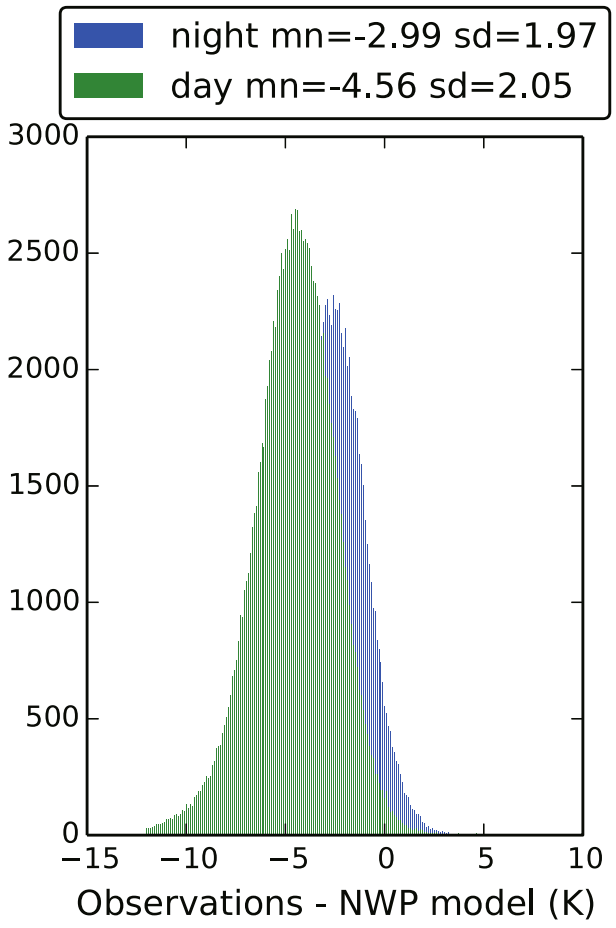

Fig. 2. Histogram of the channel 5 (23.8 GHz V-pol) observation-minus-NWP model difference for day (descending node) and night (ascending node) scenes.

the orbit track, several studies have suggested using correction schemes based on solar hours (Geer et al., 2010) or orbital angle (Booton et al., 2013). This latter scheme has been found to be effective for SSMIS and uses a Fourier series to predict the bias along the satellite track. The parameter used to denote the location of the satellite along the orbit is the orbital angle, which is the angle along the orbital plane as referenced from the intersection of the satellite's ascending node and the ecliptic plane.

In order to test whether such a scheme is appropriate for MWRI, statistics of the observations-minus-background difference were accumulated as a function of orbit angle after the observations had been screened for quality control and atmospheric conditions in which cloud effects are significant. The quality control tests follow those applied to the operational assimilation of other microwave imagers at the Met Office, such as SSMIS (Bell et al., 2008). The tests include a check that sea ice or land was not present in the field of view of the satellite. Additionally, each observation has to successfully pass a 1D-Var retrieval using channels 1–8. The retrieval includes a cloud liquid water profile and any observations with a retrieved liquid water path in excess of 40 g m^{-2} are screened out in order to remove significant cloud effects.

Finally, a test for the presence of scattering due to rain or ice particles is applied by examining the difference between the 23.8 GHz V-pol and 89 GHz V-pol channels. Observations with large positive differences are removed. Typically, after this screening, around 60% of the data over ocean remains.

Figure 3 shows a density plot of one month of observation-minus-background difference for the 23.8 V-pol GHz channel partitioned by the orbital angle. It shows a distinct variation in bias. Note the data gaps around 100° and 270°. These regions correspond to polar regions in which the data are rejected. Overlaid is a Fourier series representation of the mean bias using two Fourier terms. It suggests that the amplitude of the bias variation around the orbit for this channel is 3 K. Higher orders of Fourier terms have also been tested, but the benefits were marginal compared to the increase in computing resources. It is therefore envisaged that the four Fourier components (the cosine and sine of each term) will be used as bias predictors in the variational bias correction and updated in each 6-h model cycle using the coefficients derived from the previous cycle. The next step will be to examine the stability of the Fourier coefficients to describe the bias over a longer time period.

The pre-operational testing phase, assessing the impact of the instrument with the new orbital-angle-based correction, on the Met Office global system is planned to be conducted in early 2018.

4. Assimilation in operation

4.1. *Data processing*

MWHS-1 and MWHS-2 observations have been assimilated in operation in the Met Office global system since December and March 2016, respectively. This section describes the processing of those data.

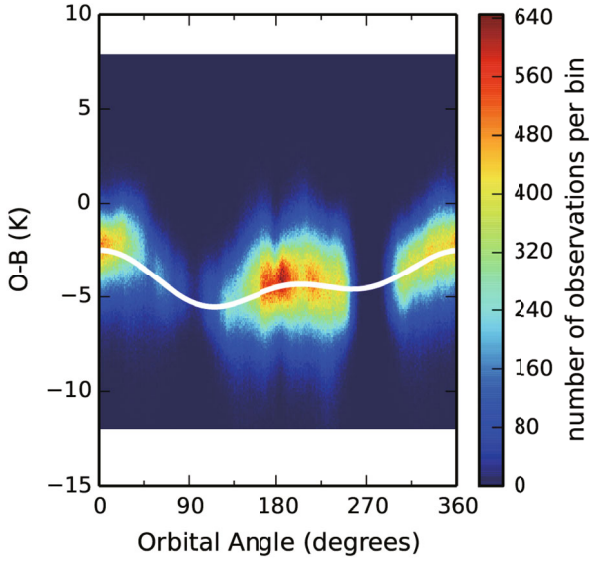

Fig. 3. FY-3C MWRI observations for the 23.8 V-pol GHz channel binned by the observation-minus-background difference and the orbital angle. Overlaid is a representation of the mean value via a Fourier series with two Fourier coefficients.

The Met Office data assimilation system operates as follows.

Firstly, raw global data for FY-3B and FY-3C are transmitted by the satellite to CMA ground stations, normally once per orbit. CMA carries out the processing to transform the raw MWHS data to files containing calibrated, geolocated brightness temperatures. Data are then sent to EUMETSAT for onward distribution to European users via EUMETCast.

At the Met Office, the brightness temperatures are spatially averaged and thinned, in line with current practice for instruments such as ATMS, MHS and SSMIS. This has the effect of reducing random instrument noise. A 2×2 average is used for MWHS-1 (giving 49 spots per scan) and a 3×3 average for MWHS-2 (30 spots per scan). The reason for the difference is that, originally, it was intended to map MWHS-2 to the Microwave Temperature Sounder-2 (MWTS-2) sample positions, similar to the process of mapping the MHS to AMSU-A. MWTS-2 has 90 spots, and a 1 in 3 sampling was to be used. When FY-3C MWTS-2 failed in 2015, the 30 spots per scan sampling was retained. The ATOVS and AVHRR Preprocessing Package (https://nwpsaf.eu/site/software/aapp/) is used to ingest the incoming data and to perform the averaging and thinning. Finally, the data are converted to BUFR format and stored in the Met Office observational database ready for use in NWP.

Secondly, a one-dimensional variational analysis (1D-Var) is performed to derive physical parameters used in the subsequent main variational process. For the MWHS instruments, atmospheric temperature and specific humidity, surface temperature, specific humidity and pressure, and skin temperature are retrieved. The retrieval uses as first guess, or background, the information coming from the 6-h forecast (T+6) of the previous assimilation cycle, interpolated at the observation location and time. Various quality controls are conducted as part of the 1D-Var analysis. Some quality controls are common to all processed instruments and include a gross error check on the observation brightness temperature and coordinates, a gross error check on the background, a convergence check, a radiative transfer error check, and a check on background departure before and after retrieval. Instrument-specific quality controls, including rejection of cloud- and rain-contaminated observations, surface type selection, or spatiotemporal screening can be applied.

The DA system at the Met Office uses a clear-sky scheme; therefore, radiances that are significantly affected by clouds must be discarded. In that respect, a cirrus cloud test discussed by Doherty et al. (2012) is applied to both MWHS instruments. The test rejects observations based on a cost function using the 183 ± 7, 183 ± 3 and 183 ± 1 GHz channels, in combination with an imposed threshold on the magnitude of the background departure at 183 ± 7 GHz. For MWHS-2, a scattering test is also applied, using the 89 and 150 GHz channels for the calculation of a scattering index, as described by English et al. (1999) and Bennartz et al. (2002). Note that those channels are used passively in 1D-Var but not assimilated. As a final pre-processing step, a 25-km 1-h window

thinning, followed by two 80-km 1-h thinnings, is applied to both instruments. Typically, 88%–92% of MWHS-1 and 79%–84% of MWHS-2 total data are rejected per cycle.

Thirdly, the data go through the main assimilation system, a hybrid incremental 4D-Var assimilation model of resolution N320L70 (~ 40 km at midlatitudes, 70 levels from surface to 80 km) and 6-h time window (Courtier et al., 1994; Rawlins et al., 2007). The forecast model used in the operational suite 37 (OS37) in 2016, when FY-3 observations were first assimilated, had a resolution N768L70 (~ 17 km at midlatitudes, 70 levels). The resolution has increased to N1280L70 (~ 10 km at midlatitudes, 70 levels) with the upgrade to the operational suite 39 (OS39) in July 2017. The implementation of OS39 also marks the transition from the radiative transfer model RTTOV 9 to RTTOV 11 (Saunders et al., 2013a). The ocean emissivity model used for the MWHS instruments is FASTEM-2 (Deblonde and English, 2000).

Since OS37 in 2016, a variational bias correction of satellite radiance observations has been used at the Met Office (Auligné et al., 2007). For MWHS, seven predictors are used, including a constant bias offset, two (200–50 hPa and 850–300 hPa) thickness predictors, and four Legendre polynomial predictors correcting residual scan biases after a static spot-dependent offset is applied prior to 4D-Var.

The operational configuration for MWHS-1 and MWHS-2 is summarized in Table 3.

4.2. *Monitoring in operation*

Continuous monitoring of satellite observations assimilated in NWP is a key task that allows the rapid detection of data anomalies, the implementation of remedies, and the feedback to data providers.

Diagnostics of satellite observations are done in brightness temperature space. During the assimilation cycle, RTTOV is used to convert model geophysical fields from the short-range forecast interpolated at the observation time and location into simulated brightness temperatures. This forward approach is better posed than in an inverse problem, which consists of comparing retrieved satellite profiles to the model, because the inverse method may have several valid solutions and therefore greater uncertainties. Similarly, the model analyses can be compared to observations instead of the forecasts, in which case the difference between observation and analysis is referred to as the residual or O-A. Note that the analysis is not independent of the observation that has already been assimilated.

Figure 4 shows, from top to bottom, the daily averaged innovation and 1σ standard deviation, the daily averaged residual and 1σ standard deviation, the difference between the innovation and residual and its standard deviation, and the number of observations as assimilated in operation, for MWHS-1 channel 4 (left) and MWHS-2 channel 13 (right), respectively.

In late November 2016, an anomaly leading to a significant increase in both MWHS-1 innovation and residual (and their respective standard deviations) was detected. Consequently, the instrument was removed from operational assimilation during the period marked by the red shading, and the report of the anomaly was fed back to CMA for investigation. The archiving of MWHS-1 data in the Met Office database was also stopped for a few days. The problem was traced back to a failure of the instrument's storage disk static random-access memory, and the backup disk has been activated instead. New bias correction coefficients, used to initiate the variational bias correction, have been generated and the instrument was reintroduced into operation in mid-January 2017.

Three other minor events have affected MWHS-1. On 14 February 2017, a small increase of a few tenths of a Kelvin in the innovation occurred because of a ground segment processing problem for the Sondeur Atmospherique du Profil d'Humidite Intertropicale par Radiometrie (SAPHIR), whose spurious data have impacted the background fit of other instruments in the system, including MWHS-1. In early March, MWHS-1 data were unavailable for a couple of days, which caused a small increase in the innovation when the number of data dropped. Finally, on 8 June 2017, a small increase in the innovation, residual, and standard deviation was detected (of maximum amplitude 0.4 K in channel 5; not shown) and fed back to the CMA. After investigation, it was found that the bias change coincided with changes in the platform energy supply scheme, adjusted to compensate for seasonal variations in the solar energy at the platform, as the eclipse pattern changes. It is not clear why these energy changes affected the instrument bias.

Away from these sudden bias changes, the MWHS-1 standard deviation is about 1.3 K (1.1 K) in the innovation (residual). Note that the standard deviation is slightly larger in channel 3 (not shown), with values up to 2.2 K (1.9 K) in the innovation (residual).

MWHS-2 time series are marked by three major bias changes occurring in May and September 2016, and Febru-

Table 3. MWHS-1 and MWHS-2 operational configuration.

Channel number		4D-Var observation error (K)		Specific rejection criteria		
MWHS-1	MWHS-2	MWHS-1	MWHS-2	Scattering test	Cirrus test	Surface
3	11	4.5	2.8028	Positive	-	Sea-ice, land
-	12	-	2.6230	Positive	-	Sea-ice, land
4	13	4	1.7717	Positive	Positive	Sea-ice, land
-	14	-	1.9913	Positive	Positive	Sea-ice, land
5	15	4	1.9981	Positive	Positive	Sea-ice, land

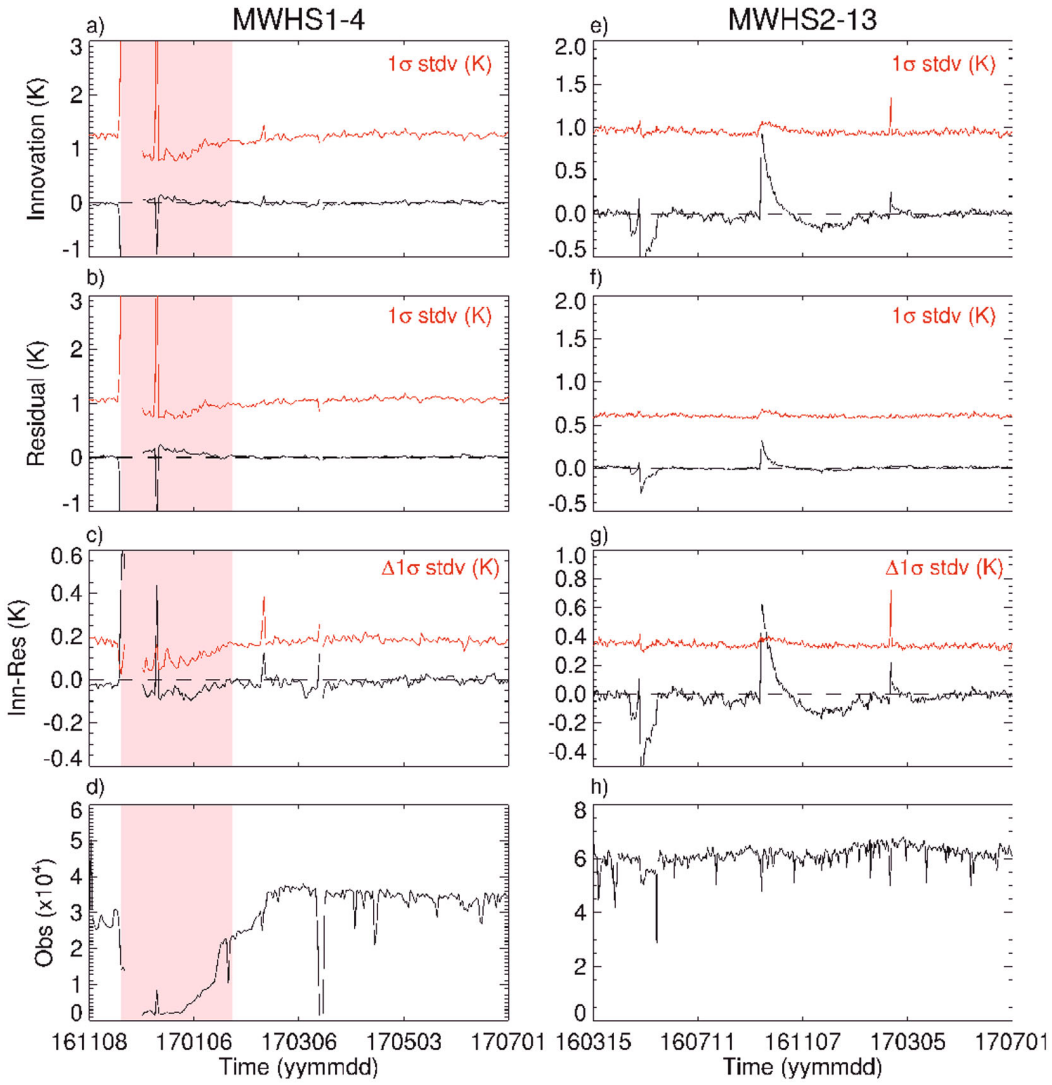

Fig. 4. The MWHS-1 (a) innovation, (b) residual, (c) difference between innovation and residual, and (d) observation count. (e–h) As in (a–d) but for MWHS-2. Red shading shows the period MWHS-1 was blacklisted.

ary 2017. The latter is a consequence of the SAPHIR ground segment problem, as described previously.

The bias changes, of opposite sign, occurring in May and in September 2016, have been related to changes in the instrument working temperature, as discussed by Lawrence et al. (2017). Over this period, modifications of the platform thermal compensation system caused the instrument environment temperature to increase by 5 K (see Lawrence et al., 2017, Fig. 3).

It is not clear, however, why systematic errors induced by the temperature changes are not removed by the onboard calibration of the instrument. The radiometric gain may have changed with the temperature, but this should not have resulted in changes to the calibrated brightness temperatures. Furthermore, the receiver nonlinearities may also have been affected, but a nonlinearity error would result in geographical bias patterns varying with the scene temperature (Lu et al., 2011b); such an effect was not observed during this period.

Apart from those spikes, the MWHS-2 standard deviation for channel 13 is 0.95 K (0.6 K) in the innovation (residual). The standard deviation is similar in channels 13–15 and slightly larger in channels 11–12 (1.5 K and 1 K in the innovation and in the residual, respectively), likely due to the different cloud screening applied to those two sets of channels (see Table 3).

Geographical patterns may also help to identify regional biases. Figure 5 shows maps of the innovation (top) and residual (middle) for MWHS-1 channel 4 (left) and MWHS-2 channel 13 (right), averaged in $1^\circ \times 1^\circ$ bins over the month of June 2017. The innovations present similar, although not identical, patterns, including a negative bias in the tropical band and a positive bias in the Southern Ocean. The negative bias is consistent with cloudy areas: the ITCZ, that is slightly north of the equator in this season, the eastern Indian Ocean and the Maritime Continent, which suggests that the bias is principally caused by the presence of unscreened

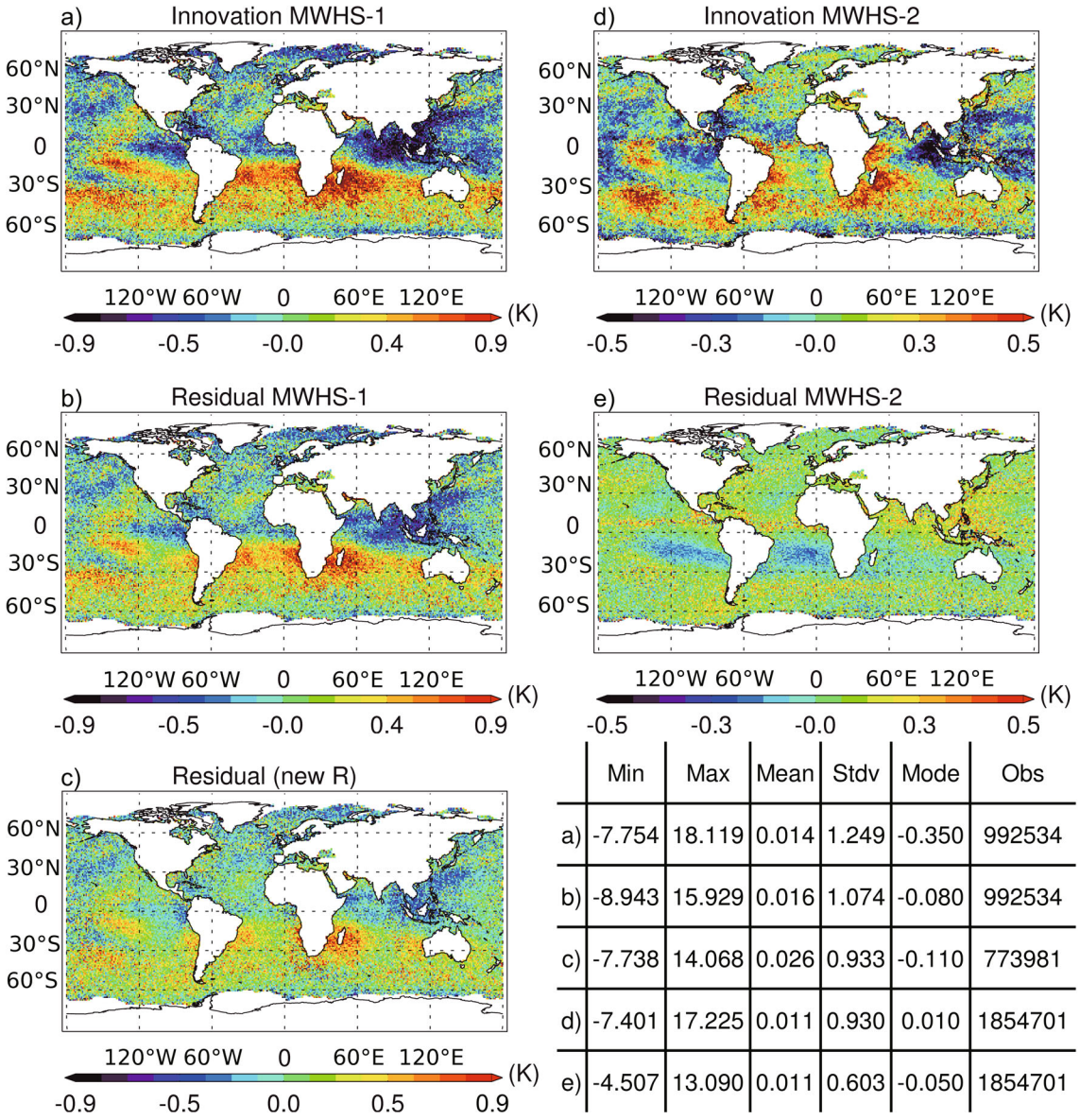

	Min	Max	Mean	Stdv	Mode	Obs
a)	-7.754	18.119	0.014	1.249	-0.350	992534
b)	-8.943	15.929	0.016	1.074	-0.080	992534
c)	-7.738	14.068	0.026	0.933	-0.110	773981
d)	-7.401	17.225	0.011	0.930	0.010	1854701
e)	-4.507	13.090	0.011	0.603	-0.050	1854701

Fig. 5. Maps of the MWHS-1 channel 4 (a) innovation, (b) residual, and (c) residual using new observation errors averaged over June 2017. (d, e) As in (a, b) but for the MWHS-2 channel 13 (d) innovation and (e) residual. The table in the bottom right gives the minimum, maximum, mean, 1σ standard deviation, mode (in K), and the number of observations for each panel.

clouds in the observations. Brightness temperatures of cloud-contaminated observations are lower (brightness temperature of the cloud top) compared to those of clear sky assumed by the model background. This means that tighter quality controls and/or the use of the 118 GHz channel's cloud-sensitivity (only for MWHS-2) might help further improve the quality of the data. The warm bias in the Southern Ocean probably results from a known bias in the model. Bodas-Salcedo et al. (2012, 2014, 2016) suggested that the global atmospheric model used at the Met Office tends to underrepresent low-level clouds above the midlatitude Southern Ocean, which results in too little solar radiation being reflected. This surplus of solar energy leads to a shortwave bias in the atmosphere model and a warm bias in sea surface temperature.

For MWHS-2, those patterns mostly disappear in the residual, whose standard deviation is driven down to 0.60 K, compared to 0.93 K in the innovation. The improvement is not as large for MWHS-1, mostly because MWHS-1 observation errors used in the 4D-Var are larger than those of MWHS-2 at equivalent frequency (i.e., greater observation errors mean less weight given to observation). In the future Met Office suite upgrade (OS40), MWHS-1 will receive observation errors equivalent to those for MWHS-2. This upcoming configuration has been used to generate the residual map shown at the bottom of Fig. 5. In this configuration, the standard deviation of the residual is reduced to 0.93 K com-

pared to 1.07 K in the residual (OS39-like configuration) and 1.25 K in the innovation.

4.3. *Operational performance*

There are several ways to estimate the impact on a system of an individual or a group of instruments. Observing System Experiments (OSEs) can be used to determine how a system reacts to the addition or the removal of instruments (Bauer, 2009).

Changes in the forecast root-mean-square error (RMSE) and forecast skill (mean-square error normalized by the mean-square error of the reference or control) can be calculated from an OSE and its control experiment. Change in the background fit for independent instruments—that is, the standard deviation of the background departures—is another metric that can be derived from OSEs.

As part of the Met Office standard pre-operational testing, several OSEs have been conducted to investigate the impact of adding MWHS-1 and MWHS-2 (separately) in a low resolution (N320L70 UM, N108/N216 4D-Var uncoupled) full global system. Those experiments are documented by Carminati et al. (2015). The impact on the forecast errors was found to be neutral overall, but benefits were shown for the background fit to the humidity-sensitive channels of independent instruments, which improved by 0.2%–2%.

Here, we investigate the combined impact of MWHS-1 and MWHS-2 with a denial experiment—an OSE where both instruments are removed from a low-resolution version of the full global system (N320 UM, N108/N216 4D-Var uncoupled). This OSE and its control have been conducted for the summer 2016, starting on 1 July and running until 30 September.

As expected from the previous experiments, the removal of FY-3 instruments has not impacted the forecast RMSE and skill (not shown). Note, this does not mean that the humidity sounders are not beneficial to the global forecasting system; rather, that the system is not optimally designed to represent those benefits. Assimilation of humidity channels has the potential to improve the model wind field. This is due to the "tracer effect", in which successive observations of the humidity field over the assimilation time-window should cause the assimilation system to adjust both the humidity and the wind fields in a consistent manner. Within the 4DVar scheme, an analysis is performed via a global minimization to reduce the discrepancy between the model first guess and the observations. In this minimization process, the full nonlinear model is run for a short forecast period; this is termed the outer loop of the minimization. Currently, the Met Office uses one cycle of the outer loop in the operational 4DVar scheme (Rawlins et al., 2007). Successive cycles of the outer loop should, in principle, improve the link between the observations and the dynamical field through successive updates of the model forecast's initial conditions. Tests of the NWP system with an increased number of outer loops are planned, with the expectation of forecast benefits to tropospheric wind, humidity and cloud fields from the humidity channels, such as those centered around 183 GHz.

A significant impact of the removal of MWHS instruments is found in the change in background fit to observations of the remaining instruments. Figure 6 shows the change in standard deviation of the innovation with respect to the control experiment for the Infrared Atmospheric Sounding Interferometer (IASI on MetOp-B), the Cross-track Infrared Sounder (CrIS on SNPP), ATMS (on SNPP), SAPHIR (Megha-Tropiques), and MHS (on NOAA19). Note the arrangement of the infrared sounder channels going from the lowest to the highest peaking temperature, and then humidity-sensitive channels.

Because the OSE is a denial experiment, we interpret the degradation of the system—here, the increase in standard deviation—as the benefit shortfall from the non-assimilation of MWHS data.

The MHS (channels 3–5), SAPHIR, and ATMS (channels 18–22) all sound the 183 GHz water vapor line. The standard deviation of their innovations all degrade by 0.2% to 1%. The overall lesser impact on SAPHIR (0.3%–0.4%) might be related to the low inclination of its orbit allowing sounding exclusively in the tropics where statistically more MWHS data are screened out due to cloud contamination.

The humidity-sensitive channels of the infrared instruments also show an increase in standard deviation by up to 0.5%, with the exception of the highermost peaking upper-tropospheric IASI channels, whose standard deviation reduces by 0.1%. It is not clear why upper-tropospheric channels are affected by the removal of MWHS data (mostly sensitive to the mid-troposphere). This might be a side effect of changes to other IASI channels. Nevertheless, this reduction is largely compensated by the increase in standard deviation at other levels.

It is worth noting that, in addition to the benefit shortfall seen at frequencies sensitive to humidity, the fit to observations for the infrared surface and tropospheric temperature channels also degrades by up to 0.7%. This illustrates how the water vapor continuum affects the observations, even at frequencies principally sensitive to temperature, and further stresses the importance of the humidity component in DA systems.

A complementary diagnostic to OSEs is the adjoint-based Forecast Sensitivity to Observation (FSO) method described by Lorenc and Marriott (2014). FSO uses the DA system to simultaneously estimate the impact of each individual piece of information in the system. FSO scores are expressed as an energy norm (J kg^{-1}). They are obtained from the sensitivity of the reduction in forecast error, which results from an assimilated observation to which is applied the adjoint of the linearized forecast model and that resulting from the 4D-Var. The FSO impact of this observation is a function of its sensitivity multiplied by its innovation.

Figure 7 (top) presents the FSO total impact per instrument type for all instruments in the system as of June 2017. Note that negative values of FSO indicate a contribution to the reduction of the 24-h forecast errors. The MWHS-2 total impact is about a fifth of that of the MHS (which includes the four MHS instruments on board MetOp-A, -B, NOAA18,

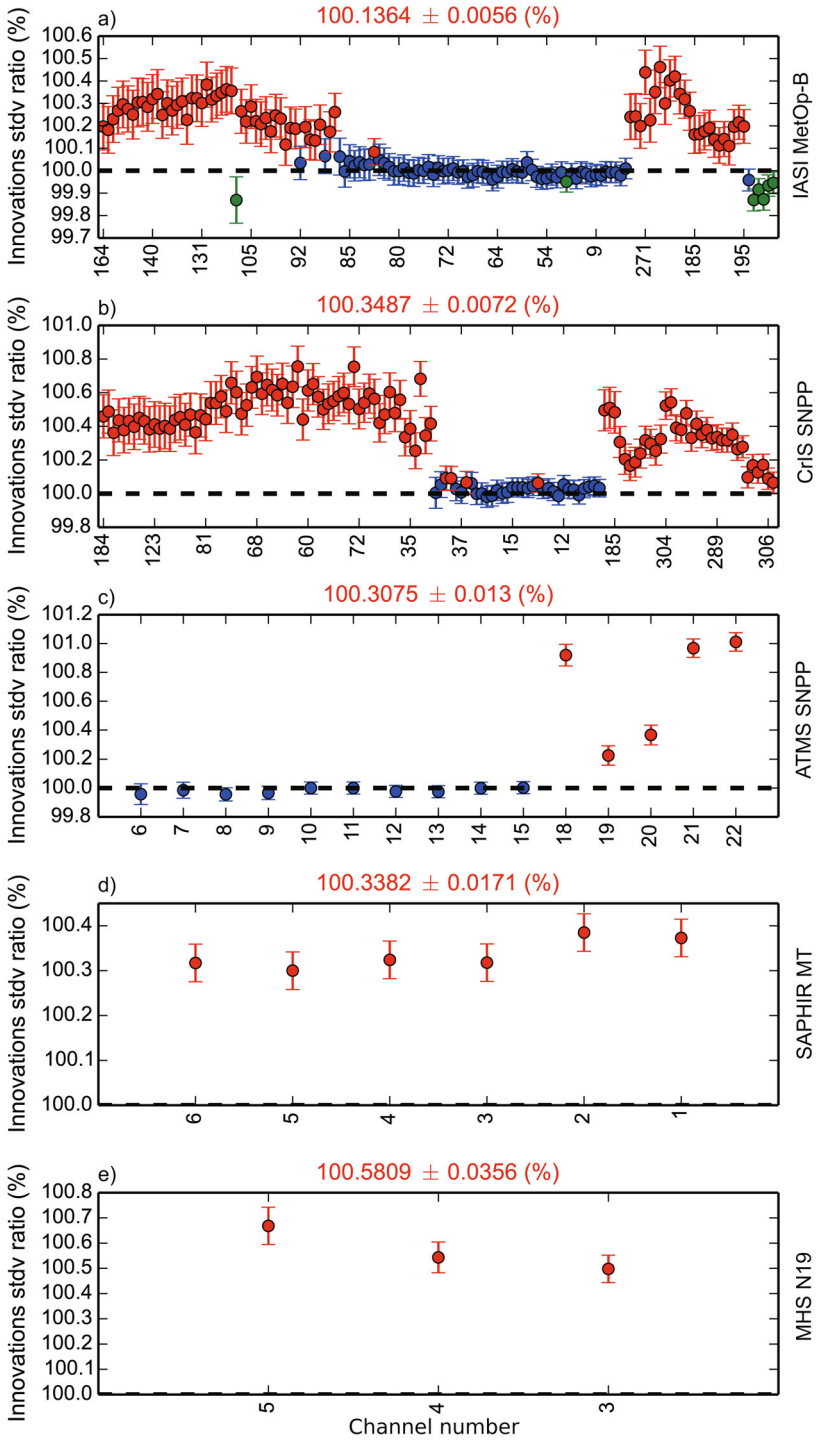

Fig. 6. Change in innovation standard deviation for (a) IASI, (b) CrIS, (c) ATMS, (d) SAPHIR, and (e) MHS, related to the denial of MWHS-1 and MWHS-2 over the period July–September 2016. Red indicates a significant increase, green a significant decrease, and blue no significant change. Note that IASI and CrIS channel numbers are not the channel numbers used in the instrument definitions, but the channel selections used at the Met Office. The red number at the top of each plot indicates the mean change across all channels ($\pm 1\sigma$).

and 19). The MWHS-1 total impact is about half of that of MWHS-2. The total impact per channel, shown in Fig. 7 (bottom) confirms that all assimilated channels of MWHS contribute, to various extents, to the reduction in forecast errors.

It is also worth noting the large benefits resulting from the assimilation of AMSR-2 data (four times that of MWHS-2). Because MWRI and AMSR-2 share similar radiometric capability, the future assimilation of MWRI data is expected to yield benefits of the same order. Microwave imagers like MWRI or AMSR-2 are sensitive to cloud and water vapor in

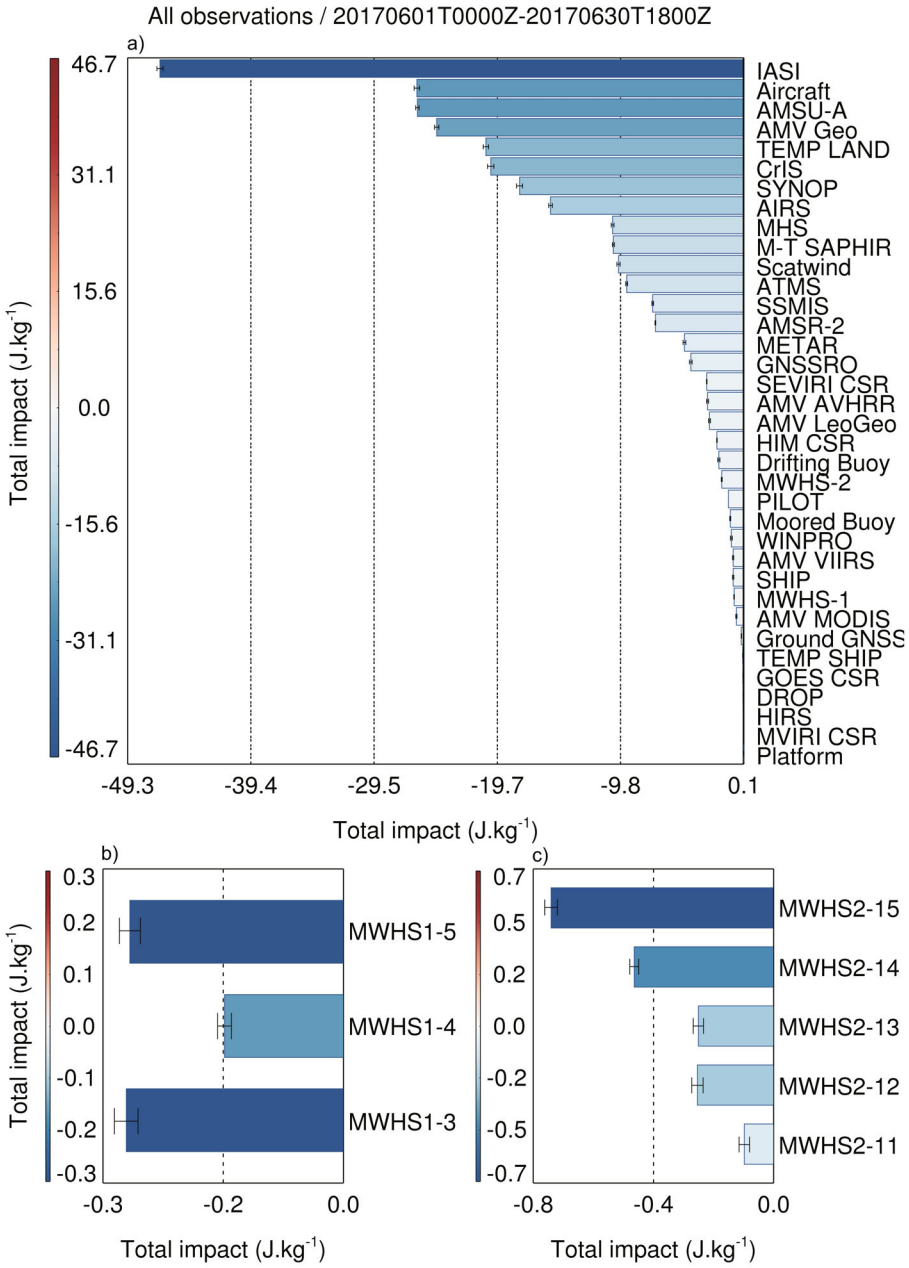

Fig. 7. (a) FSO total impact per instrument type as of June 2017. (b) FSO total impact per channel for MWHS-1 as of June 2017. (c) As in (b) but for MWHS-2.

the boundary layer. Near-surface information is essential for the correct initialization of the forecast model and only two instruments (i.e., AMSR-2 and SSMIS) are currently used in operation. In comparison, nine instruments have sounding capability in the free troposphere at 183 GHz (including MWHS-1 and -2), making the total impact per instrument (or instrument family) smaller than that of the imagers.

5. Conclusion

Since the beginning of the CSSP China program, the close collaboration between the UK Met Office, CMA-NSMC, and ECMWF has led to several landmark achievements, including the assessment of MWHS-2 and MWRI. Frequent telecommunication, visits, and dedicated workshops have helped forge strong ties with the Chinese administration, allowing the implementation of feedback loops leading to efficient investigation of anomalies in the data. This seamless communication has been crucial for the first ever assimilation in operation of Chinese polar orbiting data in the Met Office global model.

Apart from occasional sudden bias changes, observations from FY-3B MWHS-1 and FY-3C MWHS-2 were shown to be stable over time and low biased. Both instruments significantly contribute to the forecast error reduction, by 0.3%–0.6%, and improve the model background fit to observations

of independent instruments by up to 1%.

Looking forward, MWRI bias correction will be tested in pre-operational OSEs next year. It is also planned to investigate the potential use of MWHS-2 118 GHz channels. Finally, the Met Office pre-processing, 1D-Var, and 4D-Var system will shortly be prepared for the soon-to-be launched FY-3D mission, which will carry MWTS-2, MWHS-2, MWRI and the new Hyperspectral Infrared Atmospheric Sounder instruments. All these are expected to be, in due course, assimilated in operations, complementing the FY-3B MWHS-1 and FY-3C MWHS-2.

Acknowledgements. This work and its contributors (Fabien CARMINATI, Brett CANDY and William BELL) were supported by the UK–China Research & Innovation Partnership Fund through the Met Office Climate Science for Service Partnership (CSSP) China as part of the Newton Fund.

REFERENCES

Auligné, T., A. P. McNally, and D. P. Dee, 2007: Adaptive bias correction for satellite data in a numerical weather prediction system. *Quart. J. Roy. Meteor. Soc*., **133**(624), 631–642, https://doi.org/10.1002/qj.56.

Bauer, P., 2009: Observing System Experiments (OSE) to estimate the impact of observations in NWP. Conference Paper, ECMWF. [Available online from https://www.ecmwf.int/sites/default/files/elibrary/2009/7978-observing-system-experiments-ose-estimate-impact-observations-nwp.pdf]

Bell, W., and Coauthors, 2008: The assimilation of SSMIS radiances in numerical weather prediction models. *IEEE Trans. Geosci. Remote Sens*., **46**(4), 884–900, https://doi.org/10.1109/TGRS.2008.917335.

Bennartz, R., A. Thoss, A. Dybbroe, and D. B. Michelson, 2002: Precipitation analysis using the Advanced Microwave Sounding Unit in support of nowcasting applications. *Meteorological Applications*, **9**(2), 177–189, https://doi.org/10.1017/S1350482702002037.

Bodas-Salcedo, A., K. D. Williams, P. R. Field, and A. P. Lock, 2012: The surface downwelling solar radiation surplus over the Southern Ocean in the Met Office model: The role of midlatitude cyclone clouds. *J. Climate*, **25**(21), 7467–7486, https://doi.org/10.1175/JCLI-D-11-00702.1.

Bodas-Salcedo, A., P. G. Hill, K. Furtado, K. D. Williams, P. R. Field, J. C. Manners, P. Hyder, and S. Kato, 2016: Large contribution of supercooled liquid clouds to the solar radiation budget of the Southern Ocean. *J. Climate*, **29**(11), 4213–4228, https://doi.org/10.1175/JCLI-D-15-0564.1.

Bodas-Salcedo, A., and Coauthors, 2014: Origins of the solar radiation biases over the Southern Ocean in CFMIP2 models. *J. Climate*, **27**(1), 41–56, https://doi.org/10.1175/JCLI-D-13-00169.1.

Booton, A., W. Bell, and N. Atkinson, 2013: An improved bias correction for SSMIS. *Proceedings of the International TOVS Study Conference (ITSC)*, Vol. 19. [Available online from https://cimss.ssec.wisc.edu/itwg/itsc/itsc19/program/papers/10_03_booton.pdf]

Bormann, N., A. Fouilloux, and W. Bell, 2013: Evaluation and assimilation of ATMS data in the ECMWF system. *J. Geophys. Res*., **118**(23), 12 970–12 980, https://doi.org/10.1002/2013JD020325.

Carminati, F., K. Lean, and W. Bell, 2015: Assimilation of observations from the microwave humidity sounders on board China's FY-3B and FY-3C meteorological satellites. *Proceedings of the International TOVS Study Conference (ITSC)*, Vol. 20. https://cimss.ssec.wisc.edu/itwg/itsc/itsc20/papers/1_04_carminati_paper.pdf.

Chen, K. Y., S. English, N. Bormann, and J. Zhu, 2015: Assessment of *FY-3A* and *FY-3B* MWHS observations. *Wea. Forecasting*, **30**(5), 1280–1290, https://doi.org/10.1175/WAF-D-15-0025.1.

Christy, J. R., R. W. Spencer, and E. S. Lobl, 1998: Analysis of the merging procedure for the MSU daily temperature time series. *J. Climate*, **11**(8), 2016–2041, https://doi.org/10.1175/1520-0442-11.8.2016.

Courtier, P., J.-N. Thépaut, A. Hollingsworth, 1994: A strategy for operational implementation of 4D-Var, using an incremental approach. *Quart. J. Roy. Meteor. Soc*., **120**, 1367–1387, https://doi.org/10.1002/qj.49712051912.

Deblonde, G. and S. J. English, 2000: Evaluation of the FASTEM-2 fast microwave oceanic surface emissivity model. Tech. Proc. ITSC-XI, Budapest, 67–78.

Doherty, A., N. Atkinson, W. Bell, B. Candy, S. Keogh, and C. Cooper, 2012: An initial assessment of data from the Advanced Technology Microwave Sounder. Forecasting Research Technical Report, no. 569. [Available from https://library.metoffice.gov.uk]

Dong, C. H., and Coauthors, 2009: An overview of a new Chinese weather satellite FY-3A. *Bull. Amer. Meteor. Soc*., **90**(10), 1531–1544, https://doi.org/10.1175/2009BAMS2798.1.

English, S. J., J. R. Eyre, and J. A. Smith, 1999: A cloud-detection scheme for use with satellite sounding radiances in the context of data assimilation for numerical weather prediction. *Quart. J. Roy. Meteor. Soc*., **125**(559), 2359–2378, https://doi.org/10.1002/qj.49712555902.

Geer, A. J., P. Bauer, and N. Bormann, 2010: Solar biases in microwave imager observations assimilated at ECMWF. *IEEE Trans. Geosci. Remote Sens*., **48**(6), 2660–2669, https://doi.org/10.1109/TGRS.2010.2040186.

Imaoka, K., M. Kachi, M. Kasahara, N. Ito, K. Nakagawa, and T. Oki, 2010: Instrument performance and calibration of AMSR-E and AMSR2. *Proceedings of International Archives of the Photogrammetry, Remote Sensing and Spatial Information Science*, Kyoto, Japan, ISPRS, 13–18.

Kleespies, T. J. and P. Watts, 2006: Comparison of simulated radiances, Jacobians and linear error analysis for the Microwave Humidity Sounder and the Advanced Microwave Sounding Unit-B. *Quart. J. Roy. Meteor. Soc*., **132**(621C), 3001–3010, https://doi.org/10.1256/qj.05.03.

Lawrence, H., N. Bormann, Q. F. Lu, A. Geer, and S. English, 2015: An evaluation of FY-3C MWHS-2 at EMCWF. EUMETSAT/ECMWF Fellowship Programme Research Report No. 37. [Available online from https://www.ecmwf.int/sites/default/files/elibrary/2015/10668-evaluation-fy-3c-mwhs-2-ecmwf.pdf]

Lawrence, H., and Coauthors, 2017: An evaluation of FY-3C MWRI and assessment of the long-term quality of FY-3C MWHS-2 at ECMWF and the Met Office. Tech. Memo. European Centre for Medium-Range Weather Forecasts, England, 798 pp. [Available online from https://www.ecmwf.int/sites/default/files/elibrary/2017/17206-evaluation-fy-3c-mwri-and-assessment-long-term-quality-fy-3c-mwhs-2-ecmwf-and-

met-office.pdf]

Li, J., Z. K. Qin, and G. Q. Liu, 2016: A new generation of Chinese FY-3C microwave sounding measurements and the initial assessments of its observations. *Int. J. Remote Sens*., **37**(17), 4035–4058, https://doi.org/10.1080/01431161.2016.1207260.

Li, Q., 2001: Development of Chinese geostationary meteorological satellite. *Spacecraft Recovery & Remote Sensing*, **22**(1), 13–19, https://doi.org/10.3969/j.issn.1009-8518.2001.01.004. (in Chinese)

Lorenc, A. C., and R. T. Marriott, 2014: Forecast sensitivity to observations in the Met Office Global numerical weather prediction system. *Quart. J. Roy. Meteor. Soc*., **140**(678), 209–224, https://doi.org/10.1002/qj.2122.

Lu, Q. F., and W. Bell, 2014: Characterizing channel center frequencies in AMSU-A and MSU microwave sounding instruments. *J. Atmos. Oceanic Technol*., **31**(8), 1713–1732, https://doi.org/10.1175/JTECH-D-13-00136.1.

Lu, Q. F., W. Bell, P. Bauer, N. Bormann, and C. Peubey, 2011a: Characterizing the *FY-3A* microwave temperature sounder using the ECMWF model. *J. Atmos. Oceanic Technol*., **28**(11), 1373–1389, https://doi.org/10.1175/JTECH-D-10-05008.1.

Lu, Q. F., W. Bell, P. Bauer, N. Bormann, and C. Peubey, 2011b: An evaluation of FY-3A satellite data for numerical weather prediction. *Quart. J. Roy. Meteor. Soc*., **137**(658), 1298–1311, https://doi.org/10.1002/qj.834.

Lu, Q. F., H. Lawrence, N. Bormann, S. English, K. Lean, N. Atkinson, W. Bell, and F. Carminati, 2015: An evaluation of FY-3C satellite data quality at ECMWF and the Met Office. European Centre for Medium-Range Weather Forecasts Tech. Memo., England, 767 pp.

Meng Z. Z., 2004: The polar orbit meteorological satellite in China. *Engineering Sciences*, **3**, 10–15.

Muth, C., P. S. Lee, J. C. Shiue, and W. A. Webb, 2004: Advanced technology microwave sounder on NPOESS and NPP. *Proc*. 2004 *IEEE Int. Geoscience and Remote Sensing Symposium*, Anchorage, AK, USA, IEEE, https://doi.org/10.1109/IGARSS.2004.1369789.

Rawlins, F., S. P. Ballard, K. J. Bovis, A. M. Clayton, D. Li, G. W. Inverarity, A. C. Lorenc, and T. J. Payne, 2007: The Met Office global four-dimensional variational data assimilation scheme. *Quart. J. Roy. Meteor. Soc*., **133**: 347–362, https://doi.org/10.1002/qj.32.

Saunders, R. W., T. A. Blackmore, B. Candy, P. N. Francis, and T. J. Hewison, 2013b: Monitoring satellite radiance biases using NWP models. *IEEE Trans. Geosci. Remote Sens*., **51**(3), 1124–1138, https://doi.org/10.1109/TGRS.2012.2229283.

Saunders, R., and Coauthors, 2013a: RTTOV-11 science and validation report. NWPSAF-MO-TV-032, V1.1.

Tian, X. X., and X. L. Zou, 2016: An empirical model for television frequency interference correction of AMSR2 data over ocean near the U.S. and Europe. *IEEE Trans. Geosci. Remote Sens*., **54**(7), 3856–3867, https://doi.org/10.1109/TGRS.2016.2529504.

Uppala, S. M., and Coauthors, 2005: The ERA-40 re-analysis. *Quart. J. Roy. Meteor. Soc*., **131**(612), 2961–3012, https://doi.org/10.1256/qj.04.176.

Yang, H., and Coauthors, 2011: The FengYun-3 microwave radiation imager on-orbit verification. *IEEE Trans. Geosci. Remote Sens*., **49**(11), 4552–4560, https://doi.org/10.1109/TGRS.2011.2148200.

Yang, W. Z., V. O. John, X. P. Zhao, H. Lu, and K. R. Knapp, 2016: Satellite climate data records: Development, applications, and societal benefits. *Remote Sensing*, **8**(4), 331, https://doi.org/10.3390/rs8040331.

Zou, X., X. Wang, F. Weng, and G. Li, 2011: Assessments of Chinese Fengyun Microwave Temperature Sounder (MWTS) measurements for weather and climate applications. *J. Atmos. Oceanic Technol*., **28**(10), 1206–1227, https://doi.org/10.1175/JTECH-D-11-00023.1.

Zou, X. L., X. X. Tian, and F. Z. Weng, 2014: Detection of television frequency interference with satellite microwave imager observations over oceans. *J. Atmos. Oceanic Technol*., **31**(12), 2759–2776, https://doi.org/10.1175/JTECH-D-14-00086.1.

Zou, X. L., J. Zhao, F. Z. Weng, and Z. K. Qin, 2012: Detection of radio-frequency interference signal over land from FY-3B Microwave Radiation Imager (MWRI). *IEEE Trans. Geosci. Remote Sens*., **50**(12), 4994–5003, https://doi.org/10.1109/TGRS.2012.2191792.